Mathematical modeling of pathogenicity of *Cryptococcus neoformans*

Jacqueline Garcia[1], John Shea[1], Fernando Alvarez-Vasquez[1,2], Asfia Qureshi[1], Chiara Luberto[1], Eberhard O. Voit[5], and Maurizio Del Poeta[1,3,4]*

Department of [1]Biochemistry and Molecular Biology, [2]Biostatistic, Bioinformatics and Epidemiology, [3]Microbiology and Immunology, [4]Division of Infectious Diseases, Medical University of South Carolina, Charleston, SC 29425, [5] W. C. Coulter Department of Biomedical Engineering, Georgia Institute of Technology, Atlanta, Georgia, 30332, USA

SUPPORTING MATERIAL

Table of content

SECTION 1

1.1. MODEL FORMULATION

The model is adapted from a recent sphingolipid model for yeast (Alvarez-Vasquez *et al*, 2005; Alvarez-Vasquez *et al*, 2004) its governing reactions are listed in **Table S1**. The model design is accomplished in four steps. First, stoichiometric equations are formulated as shown below. Specifically, each dependent variable X_i is represented as the difference between sums of influxes and effluxes, and these can be summarily written as the difference between one aggregated influx V_i^+ and one aggregated efflux V_i^- :

$$dX_1/dt = V_{18,1} - V_{1,3} = V_1^+ - V_1^-$$

$$dX_2/dt = V_{101,2} - V_{2,3} = V_2^+ - V_2^-$$

$$dX_3/dt = (V_{1,3} + V_{2,3}) - V_{3,4} = V_3^+ - V_3^-$$

$$dX_4/dt = (V_{3,4} + V_{5,4} + V_{6,4} + V_{7,4}) - (V_{4,5} + V_{4,6} + V_{4,7} + V_{4,8}) = V_4^+ - V_4^-$$

$$dX_5/dt = V_{4,5} - V_{5,4} = V_5^+ - V_5^-$$

$$dX_6/dt = V_{4,6} - (V_{6,4} + V_{6,9}) = V_6^+ - V_6^-$$

$$dX_7/dt = V_{4,7} - V_{7,4} = V_7^+ - V_7^-$$

$$dX_8/dt = (V_{4,8} + V_{9.8} + V_{11,8} + V_{10,8}) - (V_{8,9} + V_{8,10} + V_{8,11}) = V_8^+ - V_8^-$$

$$dX_9/dt = (V_{6,9} + V_{8,9} + V_{13,9}) - (V_{9,13} + V_{9,8}) = V_9^+ - V_9^-$$

$$dX_{10}/dt = V_{8,10} - (V_{10,14} + V_{10,8}) = V_{10}^+ - V_{10}^-$$

$$dX_{11}/dt = V_{8,11} - (V_{11,15} + V_{11,8}) = V_{11}^+ - V_{11}^-$$

$$dX_{12}/dt = V_{117,12} - V_{12,125} = V_{12}^+ - V_{12}^-$$

$$dX_{13}/dt = V_{9,13} - V_{13,9} = V_{13}^+ - V_{13}^-$$

$$dX_{14}/dt = V_{10,14} - V_{14,130} = V_{14}^+ - V_{14}^-$$

$$dX_{15}/dt = V_{11,15} - V_{15,130} = V_{15}^+ - V_{15}^-$$

$$dX_{16}/dt = V_{126,16} - V_{16,125} = V_{16}^+ - V_{16}^-$$

$$dX_{17}/dt = V_{135,17} - \left(V_{17,125} + V_{17,135}\right) = V_{17}^+ - V_{17}^-$$

$$dX_{18}/dt = V_{100,18} - V_{18,1} = V_{18}^+ - V_{18}^-$$

$$dX_{19}/dt = (V_{9,13} + V_{10,14} + V_{11,15}) - V_{19,130} = V_{19}^+ - V_{19}^-$$

(Eq. S1)

These stoichiometric equations simply reflect the topology and connectivity of the pathway, but do not specify the particularities of each flux term. Thus, in the second step, the stoichiometric equations are specified as Generalized Mass Action (GMA) equations within Biochemical Systems Theory (BST) (Savageau, 1969a, b; Torres & Voit, 2002). For this step, each flux is represented as a product of power-law terms multiplied by a rate constant. Only those variables that directly affect a given dependent variable are represented in the corresponding equation. At this point, the equations are entirely symbolic, which

means that no parameter values have been specified yet. In the third step, the GMA equations are reformulated as symbolic S-system equations within BST. This step is mathematically straightforward and leads to a format that has certain advantages over the GMA form, which have been extensively discussed in the literature (Voit, 2000). While it is straightforward to write down symbolic GMA or S-system equations for all variables, a significant and complicated task is the determination of numerical parameter values. The necessary information for this determination in the fourth step of model design is derived from the literature on sphingolipids and/or *de novo* experiments. Some of this information is presented in **Table S1** (enzyme activities), **Table S2** (flux data), and **Table S3** (traditional flux representations found in the literature). The conversion of the traditional rate laws in **Table S3** into GMA and S-system equations is illustrated in the next section (Alvarez-Vasquez *et al*, 2004).

For the adaptation of the original yeast model (Alvarez-Vasquez *et al*, 2005; Alvarez-Vasquez *et al*, 2004) to a model for *C. neoformans* (*Cn*), we assume that the cytoplasmic H^+ is affected mainly by the passive influx of protons, as described in (Bowman & Slayman, 1977). The regulation of the physiological *pH* depends on the balance between cellular metabolic events and the H^+ extrusion by the H^+-ATPase (Sanders & Slayman, 1982), which is reported as closely involved in the cytoplasmic regulation of *pH* (Serrano, 1988). As described in the Text, the model demonstrates how maintenance of a constant internal *pH* relies on the manner in which H^+-ATPase is coupled with the ceramide biosynthesis and ceramide itself (Achleitner *et al*, 1999). The internal *pH* was considered to be 6.5, which is the optimal *pH* reported for Pma1 H^+-ATPase in *Cn* (Soteropoulos *et al*, 2000).

1.2. PRINCIPLES OF FLUX ESTIMATION

To illustrate the estimation procedure, we use several examples. As a very simple case, consider the proton flux J_{H+}, which may be written as

$$J_{H+} = (H_p^+ \cdot C_t \cdot M_t \cdot P_c / V), \qquad \text{(Eq. S2)}$$

where H_p^+ represents proton permeability, C_t is the capsule thickness, M_t corresponds to the melanin thickness, P_c represents the external proton concentration minus the internal proton concentration at steady state, and V is the cell volume. In this case, the flux is already given in power-law form and with the data in Table S2, the proton flux is thus calculated as:

$$J_{H+} = (8.5\mu m/min \cdot 0.16\mu m \cdot 5.41\mu m \cdot (31 - 0.31)\mu mol/l / 51.5\mu m^3) = 4.49\mu mol/min/l.$$

(Eq. S3)

As a more involved example, consider the rate functions $V_{18,1}$, $V_{1,3}$, $V_{4,5}$, $V_{4,6}$, $V_{4,7}$, $V_{8,9}$, $V_{8,10}$, $V_{8,11}$, $V_{9,13}$, $V_{9,19}$, $V_{10,14}$, $V_{10,19}$, $V_{11,19}$ and $V_{11,15}$, which all have the form of bisubstrate Michaelis-Menten rate laws and therefore need to be converted into power-laws, using specific information found in **Tables S3** and **S4**. This conversion has been demonstrated numerous times in the literature, *e.g.*, in Voit 2000 (Voit, 2000). It begins with the estimation of initial values of the dependent and independent variables, which is followed by the estimation of kinetic orders and rate constants.

In many cases of parameter estimation, data were not available for *Cn*, and we were forced to seek corresponding data from organisms that were related to *Cn* as closely as possible. Using data and parameters from a different organism is without doubt a distant secondary choice, to be used only if there is no alternative. In our particular case, such an alternative does not exist, because the needed measurements are simply not available for *Cn*. Against this background, the use of foreign data seems justified for several reasons. First, without them we could not be able to do any type of computational analysis. This would be unfortunate, because it appears to us that the modeling effort adds genuine benefit to the field. Second, it seems better to use foreign data than to rely on default assumptions; however, since we have extensive experience with default values, especially for kinetic orders, we have ensured at every step of the modeling process that the foreign data are within reasonable ranges. Third, we have subjected the model to a comprehensive sensitivity analysis. This analysis returned unremarkable results (i.e., low-magnitude sensitivities), which implies that mis-estimations in most parameter values (including those obtained from other organisms than *Cn*) do not affect the system unreasonably strong. In other words, even misjudgments of moderate magnitude are not overly influential on the state and dynamic of the integrated system. Fourth, the integration of *Cn* and non-*Cn* data seems to yield reasonable results. While this is no proof that the non-*Cn* data are acceptable, it strengthens arguments from the points above. Finally, the proposed model must clearly be considered preliminary, and we will be happy to re-estimate parameter values as soon as corresponding *Cn* data become available.

1.3. ESTIMATION OF INITIAL VALUES FOR DEPENDENT AND INDEPENDENT VARIABLES

The concentrations of X_4, X_5, X_6, X_7, X_8, X_9, X_{10}, X_{11}, X_{17} and X_{19}, were measured in our laboratory for wild type strain "H99" *Cryptococcus neoformans* under acidic conditions during the late log growth phase, as they were described in the *Materials and Methods* Section.

All dependent variables (**Table S4**) where obtained from laboratory experiments or obtained from the literature for the wild type *Cryptococcus neoformans* and when not available, from yeast references.

The independent variables $X_{100}, X_{101}, X_{102}, \ldots, X_{136}$ are unaffected by the dynamics of the system and are therefore considered constant. Numerical values for these variables are presented in **Table S1**.

1.4. ESTIMATION OF KINETIC ORDERS

Although all information is ultimately used for the S-system format, it is beneficial to begin the kinetic order estimation with the GMA format, because this representation describes all terms in the system individually, as it is also typical for traditional representations. The symbolic GMA representation is shown in **Table S6**.

Each kinetic order f_{ijk} in a GMA model is directly given as the relative partial derivative of a given flux v_{ik} with respect to X_j (Voit, 2000). Thus:

$$f_{ijk} = \frac{\partial v_{ik}}{\partial X_j} \cdot \frac{X_j}{v_{ik}}, \qquad \text{(Eq. S4)}$$

This term is to be evaluated at a nominal operating point that can be chosen arbitrarily, but usually coincides with the normal steady state of the system.

In some cases where specific information was lacking, kinetic order values were assigned a typical default value (Voit, 2000b). Such assignments are facilitated by the fact that the magnitude of a given kinetic order quantifies how strongly the corresponding variable affects a given reaction. Thus, with some biochemical insight, this magnitude can be estimated, and a subsequent sensitivity analysis can show how important the uncertainty in this estimation is. Enzymes also enter the power-law term with their own kinetic orders. In many cases, the reaction rate can be assumed to be directly proportional to enzyme activity, so that the corresponding kinetic order is known to equal 1 (Voit, 2000; Voit & Savageau, 1987).

Once the kinetic orders of the GMA model are computed, a final (mathematically trivial partial differentiation) step yields the S-system form. Specifically, the kinetic orders in the S-system equations (**Table S7**) are given by:

$$g_{i,j} = \left(\frac{\partial V_{+i}}{\partial X_j} \cdot \frac{X_j}{V_{+i}} \right)_0 ; \qquad h_{i,j} = \left(\frac{\partial V_{-i}}{\partial X_j} \cdot \frac{X_j}{V_{-i}} \right)_0 , \qquad \text{(Eq. S5)}$$

where the fluxes V could be Michaelis-Menten-type terms or sums of power-law terms in the GMA system (see Eq. S1). The numerical S-system equations for the model are presented in **Table S7**. Two specific examples of these types of derivations follow below.

***Inositol Phosphosphingolipid Phospholipase C* (Isc1, X_{119}) (Table S1).** The substrates are: **IPC-C_{26} (X_{13}), IPC-C_{24} (X_{14}) and IPC-C_{18} (X_{15}) (Table S4).** The conversion of IPC-C_{26} to phytoceramide C_{26} is catalyzed by Isc1. This yields:

$$V_{13}^{-} = v_{13,9}$$

$$v_{13,9} = \alpha_{9,13} X_{13}^{g_{9,9,13}} X_{119}^{g_{9,119,13}} X_{134}^{g_{9,134,13}}, \qquad \text{(Eq.S6)}$$

$$V_{13}^{-} = \beta_{13} X_{13}^{h_{13,13}} X_{119}^{h_{9,119}} X_{134}^{h_{9,134}}$$

$V_{max,Isc1}$ = *401.42 mg protein /l* $\cdot 0.12 \cdot 10^{-7}$ *μmol/min /mg protein* (**Table S1**) = $0.48 \cdot 10^{-5}$ *μmol/min /l*

The concentration of X_{13} was estimated from of the literature. Hechtberger and collaborators reported an IPC concentration of 155.2 nmol/mg protein in the Golgi. The total concentration of inositol containing, complex sphingolipids in the Golgi is also reported in this paper as 220.2 nmol/mg protein. The ratio between IPC-Golgi/IPC-plasma membrane is equal to 3.05 (Hechtberger *et al*, 1994). In addition, Smith and Lester reported that 74% of plasma membrane IPC contains fatty acid with 26 carbons (Smith & Lester, 1974)**.** Based on these studies, we calculated the concentration of IPC-C_{26} in the Golgi normalized with respect to total Golgi IPC as: $1 \times 0.74 \times 3.05 = 2.257$

The concentrations of IPC-C_{18} and IPC-C_{24} in the Golgi are both assumed to be 50% of the difference between IPC-C_{26} the and the total Golgi IPC. This value is estimated as $1 \times 0.26 \times 3.05 = 0.793$.

$K_{M,IPC\text{-}C26}$ = 3.57mol% (Sawai *et al*, 2000). From the equality of the GMA and S-systems at the normal operating point we calculate the kinetic order with respect to IPC-C_{26} degradation to phytoceramide C_{26} as $h_{13,9}$. This value is similar to the kinetic order with respect to phytoceramide C_{26} biosynthesis from IPC-C_{26}.

$$h_{13,13} = \frac{\partial(V_{13}^{-})}{\partial X_{13}} \cdot \frac{X_{13}}{V_{13}^{-}} =$$

$$= \frac{\partial}{\partial X_{13}} \left[X_{119} \left(\frac{X_{13}}{X_{13} + K_{M,IPCC26}} \right) \right] \cdot \frac{X_{13}}{V_{13}^{-}}, \qquad \text{(Eq.S7)}$$

$$h_{13,13} = \frac{\partial V_{13}^{-}}{\partial X_{13}} \cdot \frac{X_{13}}{V_{13}^{-}} = 0.6126$$

$$h_{13,13} = g_{9,9,13}$$

***Inositol phosphorylceramide synthase* (*Ipc1 Synthase,* X_{121}) (Table S1).** The substrates are: **Phytoceramide-C_{26} (X_9), Phytoceramide-C_{24} (X_{10}), Phytoceramide-C_{18} (X_{11}) (Table S4).** Ipc1 (X_{121})

catalyzes the IPC-C_{26} conversion in the ceramide degradation pathway with phytoceramide C_{26} as substrate. The GMA and S-system terms are:

$$V_{13}^{+} = v_{9,13}$$

$$v_{9,13} = \beta_{9,13} X_9^{h_{9,9,13}} X_{120}^{h_{9,120,13}} X_{121}^{h_{9,121,13}} X_{127}^{h_{9,127,13}}, \qquad \text{(Eq. S8)}$$

$$V_{13}^{+} = \alpha_{13} X_9^{g_{13,9}} X_{120}^{g_{13,120}} X_{121}^{g_{13,121}} X_{127}^{g_{13,127}}$$

$V_{max,Ipc1} = 401.42\ mg\ protein\ /l \cdot 0.000035\ \mu mol/min\ /mg\ protein$ (**Table S1**) = 0.014 $\mu mol/min\ /l\ X_9$ = 0.166 (**Table S4**), X_{120} = 4.54 mol% (Wu *et al*, 1995) $K_{M,Phyto\text{-}C26}$ = 1.35 mol% (Fischl *et al*, 2000a) and $K_{M,PI}$ = 5 mol% (Fischl *et al*, 2000b) . With this information we compute the kinetic order as:

$$g_{13,9} = \frac{\partial V_{9,13}}{\partial X_9} \cdot \frac{X_9}{V_{9,13}} =$$

$$= \frac{\partial}{\partial X_9}\left[X_{121} \left(\frac{X_9}{X_9 + K_{M,PhytoC26}} \right) \cdot \left(\frac{X_{120}}{X_{120} + K_{M,PI}} \right) \right] \cdot \frac{X_9}{V_{9,13}}, \qquad \text{(Eq.S9)}$$

$$g_{13,9} = \frac{\partial V_{9,13}}{\partial X_9} \cdot \frac{X_9}{V_{9,13}} = 0.8905$$

$$g_{13,9} = h_{9,121,13}$$

1.5. PHYTOCERAMIDE AFFECTS Pma1 (X_{12}) ACTIVITY

According to our experimental results under acidic *pH* (**Table 4**), Isc1 (X_{119}) mutants exhibit decreased Phytoceramide C_{26} levels, and loss of Isc1 and down-regulation of Ipc1 sensitize *C. neoformans* to the Pma1 inhibitor ebselen (**Table 2**), while Ipc1 (X_{121}) down-regulation at acidic *pH* produces an increase in Phytoceramide C_{26} (**Table 4**).

The rate of change of Pma1 (X_{12}) with respect to its assembly is expressed in the model as:

$$V_{12}^{+} = \alpha_{12} X_{13}^{g_{12,13}} X_9^{g_{12,9}} X_{119}^{g_{12,119}} X_{121}^{g_{12,121}} X_{117}^{g_{12,117}} X_{118}^{g_{12,118}} \qquad \text{(Eq. S10)}$$

where some of the kinetic orders are equivalent in the GMA and S-system formats:

Constraints between kinetic orders

S-system				GMA
$g_{12,9}$	=	$g_{13,9}$	=	$h_{9,121,13}$
$g_{12,13}$	=	$h_{13,13}$	=	$g_{9,13,13}$
$g_{12,121}$	=	$h_{9,121}$		
$g_{12,119}$	=	$h_{13,119}$	=	$g_{9,119,13}$

(Eq. S11)

1.6. Pma1 TURNOVER

Cryptococcus neoformans H99 microarray results (Fan *et al*, 2005) were used as an additional means of parameter estimation in the model, under the assumption that changes in gene expression correspond directly to changes in the corresponding enzyme activities (Voit, 2002). Thus, we used supplementary material in Fan *et al*. (Fan *et al*, 2005) describing up-regulation of mRNA corresponding to H^+ATPase, a potential phospholipid-transporting ATPase, ATP synthase, and Sec61p genes during murine macrophage infection. This condition is similar to the internalization of the fungus within the macrophages after 24 hours (**Table S8**). Genes involved in lipid metabolism, such as IPC1, are indeed induced in Cn found within macrophages (Fan *et al*, 2005).

The degradation term V_{12}^- in our model includes the potential phospholipid-transporting ATPase as well as ATPase itself. Thus, we specify:

$$V_{12}^- = \beta_{12} X_{12}^{h_{12,12}} X_{125}^{h_{12,125}} \qquad \text{(Eq. S12)}$$

The kinetic order $h_{12,12}$ characterizes the degradation of Pma1 (X_{12}):

$V_{12}(X_{12}) = X_{12} \cdot [mRNA]$ (Potential phospholipids transporting ATPase),

$$h_{12,12} = \frac{\partial\left(X_{12} \cdot [mRNA]\right)}{\partial X_{12}} \cdot \frac{X_{12}}{\left(X_{12} \cdot [mRNA]\right)} = 1 \qquad \text{(Eq.S13)}$$

The activity of ATPase is modeled as the independent variable X_{125}

$$X_{125} = V_{max,ATPase} \cdot [ATP], \qquad \text{(Eq. S14)}$$

Thus, $h_{12,125} = 1$

1.7. ESTIMATION OF RATE CONSTANTS

The kinetic orders for all fluxes were calculated as shown in the previous sections and with information exhibited in **Tables S3** and **S4**. Thus given all kinetic orders, the rate constants were computed in the final step of model design by recognizing that all original flux terms and the corresponding power-law terms are equivalent at the chosen operating point. Therefore, recalling Equation 2 of the main text, we obtain:

$$\alpha_i = \left(V_i^+\right)_0 \prod_{j=1}^{n+m}\left(X_{j0}\right)^{-g_{ij}}, \quad \beta_i = \left(V_i^-\right)_0 \prod_{j=1}^{n+m}\left(X_{j0}\right)^{-h_{ij}}, \quad i = 1,\ldots,n \qquad \text{(Eq. S15)}$$

As an example, consider flux

$$V_1^- = V_{1,3} = \beta_1 X_1^{h_{1,1}} X_2^{h_{1,2}} X_{108}^{h_{1,108}} \qquad \text{(Eq. S16)}$$

for which β_1 the rate constant is calculated as:

$$\beta_1 = V_{1,3} \Big/ X_1^{h_{1,1}} X_2^{h_{1,2}} X_{108}^{h_{1,2}} =$$
$$= 0.1404 \Big/ \left(0.2^{0.5} \cdot 2.6^{0.071} \cdot 0.014^{1} \right) = 20.95 \qquad \text{(Eq. S17)}$$

Table S7 shows the numerical S-system equations with all kinetic orders and rate constants specified. Values of the independent variables are shown in **Table S9**.

SECTION 2

CONSTRAINTS

2.1 CONSTRAINTS REGARDING PROTONS IN THE MEDIUM

The relationships between cell charge, virulence and phagocytosis in microbial pathogens are complex and poorly understood. Both melanin and the microbe's polysaccharide capsule contribute to the cellular negative charge, with the capsule being the more significant contributor (Garcia-Rivera *et al*, 2005; Nosanchuk & Casadevall, 1997). One crucial component of cellular charge is the *Z* potential, which is defined as the potential gradient produced across the interface between a boundary liquid in contact with a solid. For the encapsulated strain 24067, grown with L-dopa at *pH*=7.3 and with 29.4 mM of KH_2PO_4 in the medium, the *Z* potential was measured as –24.42 mV (Nosanchuk & Casadevall, 1997). Furthermore, the stoichiometry of H^+/ATP for Pma1 is 1, *i.e.*, one proton is extruded per molecule of ATP hydrolyzed (van der Rest *et al*, 1995).

The *pH* of a solution is the negative logarithm of the hydrogen ion (H^+) concentration (whose molarity is in moles per liter). The external acidic *pH* in the model is assumed as 4.5, which mimics the reported *pH* of phagolysosomes in alveolar macrophages (Levitz *et al*, 1999). The proton electrochemical gradient can be represented by the following relationship:

$$\frac{\Delta\mu_{H^+}}{F} = -Z\Delta pH + \Delta\psi(mv), \qquad \text{(Eq. S18)}$$

Where, $\Delta\psi$ represents the electrical potential across the membrane, $\Delta\mu_{H^+}$ represents the electrochemical gradient, Z is the Z potential and F is the Faraday constant. The *pH* difference is

$$\Delta pH = pH_i - pH_{ext.}, \qquad \text{(Eq. S19)}$$

where pH_i and $pH_{ext.}$ correspond to the internal and external *pH* respectively.

Starting with 2 mmol/g of K^+ in the medium, the membrane potential $\Delta\psi$ and the electrochemical gradient $\Delta\mu_{H^+}$ remain approximately constant in spite of increasing medium K^+ concentrations (Bakker & Mangerich, 1981). This observation renders it possible to represent the *pH* difference as a constant *A* in the equation

$$pH_i - pH_{ext.} = \frac{\Delta\mu_{H+} - F\Delta\psi}{24.42F}, \qquad \text{(Eq. S20)}$$

$$A = \frac{\Delta\mu_{H+} - F\Delta\psi}{24.42F}, \qquad \text{(Eq. S21)}$$

After substitution and rearrangements of the equation for $pH_{ext.}$, one obtains:

$$-pH_{ext.} = A - pH_i, \qquad \text{(Eq. S22)}$$

Exponentiation of both sides yields:

$$10^{-pH_{ext.}} = 10^{A-pH_i}, \qquad \text{(Eq. S23)}$$

and substituting

$$B = 10^A, \qquad \text{(Eq. S24)}$$

leads to a representation of the medium proton concentration as

$$\left[H^+_{ext.}\right] = \left[H^+_{i}\right] \cdot B, \qquad \text{(Eq. S25)}$$

This equation can be expressed in power law format as

$$X_{126} = \gamma X_{16}^{f_{126,16}} \qquad \text{(Eq. S26)}$$

where the kinetic order $f_{126,16}$ is derived from the general Equation S4 given in Section 1. In our particular case, X_{126} is the external proton concentration and X_{16} the cytoplasmatic proton concentration. Thus,

$$f_{126,16} = \frac{\partial V_{126}}{\partial X_{16}} \cdot \frac{X_{16}}{X_{126}} = 1 \qquad \text{(Eq. S27)}$$

2.2 CONSTRAINTS REGARDING ADENOSINE PHOSPHATE

The variables *ADP* and *AMP* are constrained by their relationships with ATP. Specifically, the total adenosine phosphate pool is written as

$$X_T = X_{ATP} + X_{ADP} + X_{AMP}, \qquad \text{(Eq. S28)}$$

and we invoke the relationship within the adenosine phosphate pool reported in (Meixner-Monori *et al*, 1985) as:

$$X_{AMP} = \frac{X_{ATP} + X_{ADP}}{4}, \qquad \text{(Eq. S29)}$$

Substituting X_{AMP} into X_T, we obtain:

$$X_{ADP} = \frac{4}{5} X_T - X_{ATP} \qquad \text{(Eq. S30)}$$

In the power-law formalism, X_{ADP} can be expressed as:

$$X_{ATP} = \gamma_{ADP} X_t^{f_{ADP,T}} X_{ATP}^{f_{ADP,ATP}}, \qquad \text{(Eq. S31)}$$

where,

$$f_{ATP,T} = \frac{\partial X_{ADP}}{\partial X_T} \cdot \frac{X_T}{X_{ADP}} = \frac{4}{5} \cdot \frac{X_T}{X_{ADP}} \qquad \text{(Eq. S32)}$$

$$f_{ADP,ATP} = \frac{\partial X_{ADP}}{\partial X_{ATP}} \cdot \frac{X_{ATP}}{X_{ADP}} = -\frac{X_{ATP}}{X_{ADP}} \qquad \text{(Eq. S33)}$$

SECTION 3

LOGARITHMIC GAIN ANALYSIS

3.1 Metabolite gains

The logarithmic gain of metabolite concentration X_i with respect to a change in an independent variable (*e.g.*, enzyme) X_j is defined as:

$$L(X_i, X_j) = (\partial X_i / \partial X_j)(X_j / X_i) = \partial(\log X_i) / \partial(\log X_j), \qquad \text{(Eq. S34)}$$

(Voit, 2000). The effects of enzymes on phytoceramide biosynthesis and it metabolism are shown in the **Figures S2** and **S3**. **Figure S2** shows logarithmic gains with respect to metabolite concentrations, separating positive and negative influences. Similarly, **Figure S3** shows logarithmic gains with respect to fluxes, which are defined in analogy with Eq. S34 as the fold change in a flux V_i divided by the fold change in an independent variable X_j. (see Eq. S35). While Figures **S2A,B** and **S3A,B** sum the gains over affected and effecting variables, **Figures S2C** and **S3C** show the magnitude of each gain individually.

The independent variables that have the most positive influence on metabolite concentrations are external serine and palmitate; X_{100}, X_{102}, respectively. This is not surprising, because these variables are the system's precursors that supply most of the input material. The following independent variables also have a relatively strong effect on the system: dihydroceramide synthase (X_{112}), serine transport (X_{103}), fatty acid (C_{18}-CoA) (X_{106}), hydroxylase (X_{115}) and Ipc1(X_{121}) inositol phosphorylceramide synthase. In particular, any increases in the activities of these enzymes will noticeably raise phytoceramide levels.

Independent variables with the largest negative effects on metabolite concentrations are: fatty acid (C_{24}-CoA) (X_{107}), serine palmitoyltransferase (X_{108}), dihydroceramide ceramidase, (X_{110}), phyto-ceramidase (X_{113}), hydroxylase (X_{114}). Any increase in their activities will lead to reductions in phytoceramide metabolism.

Generally, there are significant differences in the contributions of the independent variables on the system. This is evident in the two-dimensional projection of **Figure S2A**. As an illustration, a perturbation in Ipc1 (X_{121}) activity has a more significant effect than a perturbation in Isc1 on inositol phosphorylceramide C_{26} (X_{13}) with a value of $L(X_{13}, X_{121})$ = 1.62 and IPC-C_{18} (X_{15}), inositol phosphorylceramide C_{18} with a value of $L(X_{15}, X_{121})$ = -1.66. A perturbation in Isc1 has a negative effect on IPC-C_{26} (X_{13}) with value of $L(X_{13}, X_{119})$ = -1.63.

The two-dimensional projection **Figure S2B** shows metabolite concentrations that are most affected positively by changes in independent variables. They are: IPC-C_{26} (X_{13}), inositol phosphorylceramide C_{26}, IPC-C_{18} (X_{15}), inositol phosphorylceramide C_{18}, serine (X_2), Dihydro-C18 (X_7), dihydroceramide C_{18}, Phyto-C_{26} (X_9), phytoceramide-C_{26}, Phyto-C_{18} (X_{11}), phytoceramide-C_{18}, Dihydro-C_{24} (X_5), dihydroceramide C_{24}, Pma1 (X_{12}), and DAG (X_{19}), *sn*-1,2-diacylglycerol. The largest negative influences are seen in IPC-C_{26} (X_{13}), serine (X_2), PHS (X_8), phytosphingosine, IPC-C_{18} (X_{15}), Dihydro-C_{18} (X_7), intracellular Protons (X_{16}) and Phyto-C_{26} (X_9).

As a specific illustration, the largest log gains associated with metabolite X_9 are associated with the following independent variables: positive gain of $L(X_9, X_{112})$ =1.02, negative gain of $L(X_9, X_{113})$ = -1.99 and an insignificant gain of $L(X_9, X_{121})$ = 1.9 E-3 with respect to Ipc1. By contrast, X_{13} is most strongly affected by changes in X_{112} and X_{113}, with values of $L(X_{13}, X_{112})$ = 1.49 and $L(X_{13}, X_{113})$ = -2.89, respectively.

Noteworthy log gains with respect to Pma1 (X_{12}) are $L(X_{12}, X_{112})$ = 1.82, $L(X_{12}, X_{113})$ = -3.54 and $L(X_{12}, X_{121})$ = 1.99. Overall, the log gains with respect to Pma1 are predominantly positive (see **Figure S2A**).

Several metabolites are unaffected by changes in Isc1(X_{119}) or Ipc1(X_{121}). Examples are $L(X_1\text{-}X_{12}, X_{119}) = L(X_{14}, X_{119}) = L(X_{15}, X_{119}) = L(X_{18}, X_{119}) = L(X_{19}, X_{119}) = L(X_1\text{-}X_7, X_{121}) = L(X_{17}, X_{121}) = L(X_{18}, X_{121}) = 0$ (**Figure S2C**).

3.2 FLUX GAINS

Logarithmic flux gains refer to changes in any of the V_i with respect to changes in an independent variable X_j. They are defined as:

$$L(V_i, X_j) = (\partial V_i / \partial X_j)(X_j / V_i) = \partial(\log V_i) / \partial(\log X_j), \qquad \text{(Eq. S35)}$$

(cf. Eq. S34 and Voit, 2000b). Flux gains are shown in **Figure S3A**, where they are summed over all fluxes V_i for a given independent variable X_j, and in **Figure S3B**, where they are summed for each independent variable. As an example, **Figure S3B** shows how a perturbation in Ipc1 will increase the steady-state flux through Pma1.

The contribution of each independent variable on each steady-state flux is exhibited in the three-dimensional plot of **Figure S3C.** One can easily see that almost all fluxes are strongly affected by perturbations in the initial steps of ceramide biosynthesis, and in particular in: palmitate transport, (X_{102}), serine transport, (X_{103}), palmitate external (X_{100}).

Changes in ceramide biosynthesis can be quite different, dependent on which independent variable is perturbed. The fluxes through Pal-CoA, Serine, and KDHS are unaffected by any perturbations in the variables $X_{104},\ldots,X_{115}$. Also, changes in the independent variables $X_{116},\ldots,X_{136}$ do not affected the fluxes through variables $X_1,..,X_7$. By contrast, the fluxes throughPma1, H^+, and ATP are affected by changes in several independent variables; most important are the positive log gains $L(V_{12}, X_{112})$= 1.82, $L(V_{12}, X_{115})$ = 1.69, $L(V_{12}, X_{121})$= 1.99 and the negative gains $L(V_{12}, X_{110})$= -1.69, $L(V_{12}, X_{113})$ = -3.54, $L(V_{12}, X_{115})$= 1.69, and $L(V_{12}, X_{134})$= -1.

Noteworthy products of phytoceramide C_{26} metabolism are phytosphingosine (X_8) and IPC-C_{26} (X_{13}), which are affected by Ipc1, X_{121} with the logarithmic gains $L(V_8, X_{121})$= -0.0058 and $L(V_{13}, X_{121})$= 0.99. The corresponding alternative fluxes through phytoceramide C_{24} and phytoceramide C_{18} at the ceramide branch are less affected: $L(V_{10}, X_{121})$ = - 0.0058 and $L(V_{11}, X_{121})$ = - 0.0058.

An increase in Isc1 (X_{121}) results in an increase in ATP with a log gain of $L(V_{17}, X_{119})$ = 0.63. This enzyme has small log gains with respect to all other fluxes in the model.

SUPPLEMENTARY REFERENCES

Achleitner G, Gaigg B, Krasser A, Kainersdorfer E, Kohlwein SD, Perktold A, Zellnig G, Daum G (1999) Association between the endoplasmic reticulum and mitochondria of yeast facilitates interorganelle transport of phospholipids through membrane contact. *Eur J Biochem* **264:** 545-553.

Akhter S, McDade HC, Gorlach JM, Heinrich G, Cox GM, Perfect JR (2003) Role of alternative oxidase gene in pathogenesis of Cryptococcus neoformans. *Infect Immun* **71:** 5794-5802.

Alvarez-Vasquez F, Sims KJ, Cowart LA, Okamoto Y, Voit EO, Hannun YA (2005) Simulation and validation of modelled sphingolipid metabolism in *Saccharomyces cerevisiae*. *Nature* **433:** 425-430.

Alvarez-Vasquez F, Sims KJ, Hannun YA, Voit EO (2004) Integration of kinetic information on yeast sphingolipid metabolism in dynamical pathway models. *J Theor Biol* **226:** 265-291.

Arselin G, Giraud MF, Dautant A, Vaillier J, Brethes D, Coulary-Salin B, Schaeffer J, Velours J (2003) The GxxxG motif of the transmembrane domain of subunit e is involved in the dimerization/oligomerization of the yeast ATP synthase complex in the mitochondrial membrane. *Eur J Biochem* **270:** 1875-1884.

Averet N, Aguilaniu H, Bunoust O, Gustafsson L, Rigoulet M (2002) NADH is specifically channeled through the mitochondrial porin channel in Saccharomyces cerevisiae. *J Bioenerg Biomembr* **34:** 499-506.

Bakker EP, Mangerich WE (1981) Interconversion of components of the bacterial proton motive force by electrogenic potassium transport. *J Bacteriol* **147:** 820-826.

Bowman BJ, Slayman CW (1977) Characterization of plasma membrane adenosine triphosphatase of Neurospora crassa. *The Journal of biological chemistry* **252:** 3357-3363.

Eisenman HC, Nosanchuk JD, Webber JB, Emerson RJ, Camesano TA, Casadevall A (2005) Microstructure of cell wall-associated melanin in the human pathogenic fungus Cryptococcus neoformans. *Biochemistry* **44:** 3683-3693.

Faergeman NJ, Knudsen J (1997) Role of long-chain fatty acyl-CoA esters in the regulation of metabolism and in cell signalling. *Biochem J* **323 (Pt 1):** 1-12.

Fan W, Kraus PR, Boily MJ, Heitman J (2005) Cryptococcus neoformans Gene Expression during Murine Macrophage Infection. *Eukaryot Cell* **4:** 1420-1433.

Fein JE, MacLeod RA (1975) Characterization of neutral amino acid transport in a marine pseudomonad. *J Bacteriol* **124:** 1177-1190.

Fischl AS, Liu Y, Browdy A, Cremesti AE (2000a) Inositolphosphoryl ceramide synthase from yeast. *Methods Enzymol* **311:** 123-130.

Fischl AS, Liu Y, Browdy A, Cremesti AE (2000b) Inositolphosphoryl ceramide synthase from yeast. *Methods Enzymol* **311:** 123-130.

Garcia-Rivera J, Chang YC, Kwon-Chung KJ, Casadevall A (2004) Cryptococcus neoformans CAP59 (or Cap59p) is involved in the extracellular trafficking of capsular glucuronoxylomannan. *Eukaryot Cell* **3:** 385-392.

Garcia-Rivera J, Eisenman HC, Nosanchuk JD, Aisen P, Zaragoza O, Moadel T, Dadachova E, Casadevall A (2005) Comparative analysis of Cryptococcus neoformans acid-resistant particles generated from pigmented cells grown in different laccase substrates. *Fungal Genet Biol* **42:** 989-998.

Grilley MM, Stock SD, Dickson RC, Lester RL, Takemoto JY (1998) Syringomycin action gene SYR2 is essential for sphingolipid 4-hydroxylation in Saccharomyces cerevisiae. *The Journal of biological chemistry* **273:** 11062-11068.

Guillas I, Kirchman PA, Chuard R, Pfefferli M, Jiang JC, Jazwinski SM, Conzelmann A (2001) C26-CoA-dependent ceramide synthesis of Saccharomyces cerevisiae is operated by Lag1p and Lac1p. *Embo J* **20:** 2655-2665.

Hechtberger P, Zinser E, Saf R, Hummel K, Paltauf F, Daum G (1994) Characterization, quantification and subcellular localization of inositol-containing sphingolipids of the yeast, Saccharomyces cerevisiae. *Eur J Biochem* **225:** 641-649.

Heung LJ, Luberto C, Plowden A, Hannun YA, Del Poeta M (2004) The sphingolipid pathway regulates protein kinase C 1 (Pkc1) through the formation of diacylglycerol (DAG) in *Cryptococcus neoformans*. *J Biol Chem* **279:** 21144-21153.

Kamiryo T, Parthasarathy S, Numa S (1976) Evidence that acyl coenzyme A synthetase activity is required for repression of yeast acetyl coenzyme A carboxylase by exogenous fatty acids. *Proc Natl Acad Sci U S A* **73:** 386-390.

Kastanos EK, Woldman YY, Appling DR (1997) Role of mitochondrial and cytoplasmic serine hydroxymethyltransferase isozymes in de novo purine synthesis in Saccharomyces cerevisiae. *Biochemistry* **36:** 14956-14964.

Kelley MJ, Bailis AM, Henry SA, Carman GM (1988) Regulation of phospholipid biosynthesis in Saccharomyces cerevisiae by inositol. Inositol is an inhibitor of phosphatidylserine synthase activity. *The Journal of biological chemistry* **263:** 18078-18085.

Kihara A, Igarashi Y (2004) FVT-1 is a mammalian 3-ketodihydrosphingosine reductase with an active site that faces the cytosolic side of the endoplasmic reticulum membrane. *The Journal of biological chemistry* **279:** 49243-49250.

Knudsen J, Jensen MV, Hansen JK, Faergeman NJ, Neergaard TB, Gaigg B (1999) Role of acylCoA binding protein in acylCoA transport, metabolism and cell signaling. *Mol Cell Biochem* **192:** 95-103.

Levitz SM, Nong SH, Seetoo KF, Harrison TS, Speizer RA, Simons ER (1999) *Cryptococcus neoformans* resides in an acidic phagolysosome of human macrophages. *Infect Immun* **67:** 885-890.

Lodge JK, Johnson RL, Weinberg RA, Gordon JI (1994) Comparison of myristoyl-CoA:protein N-myristoyltransferases from three pathogenic fungi: *Cryptococcus neoformans, Histoplasma capsulatum*, and *Candida albicans*. *J Biol Chem* **269:** 2996-3009.

Mao C, Xu R, Bielawska A, Obeid LM (2000) Cloning of an alkaline ceramidase from Saccharomyces cerevisiae. An enzyme with reverse (CoA-independent) ceramide synthase activity. *The Journal of biological chemistry* **275:** 6876-6884.

Matsuyama S, Reed JC (2000) Mitochondria-dependent apoptosis and cellular pH regulation. *Cell death and differentiation* **7:** 1155-1165.

Meixner-Monori B, Kubicek CP, Habison A, Kubicek-Pranz EM, Rohr M (1985) Presence and regulation of the alpha-ketoglutarate dehydrogenase multienzyme complex in the filamentous fungus Aspergillus niger. *J Bacteriol* **161:** 265-271.

Merrill AH, Jr., Wang E, Mullins RE (1988) Kinetics of long-chain (sphingoid) base biosynthesis in intact LM cells: effects of varying the extracellular concentrations of serine and fatty acid precursors of this pathway. *Biochemistry* **27:** 340-345.

Nosanchuk JD, Casadevall A (1997) Cellular charge of Cryptococcus neoformans: contributions from the capsular polysaccharide, melanin, and monoclonal antibody binding. *Infect Immun* **65:** 1836-1841.

Ohkusu M, Raclavsky V, Takeo K (2004) Induced synchrony in Cryptococcus neoformans after release from G2-arrest. *Antonie Van Leeuwenhoek* **85:** 37-44.

Pinto WJ, Srinivasan B, Shepherd S, Schmidt A, Dickson RC, Lester RL (1992a) Sphingolipid long-chain-base auxotrophs of *Saccharomyces cerevisiae*: genetics, physiology, and a method for their selection. *J Bacteriol* **174:** 2565-2574.

Pinto WJ, Wells GW, Lester RL (1992b) Characterization of enzymatic synthesis of sphingolipid long-chain bases in Saccharomyces cerevisiae: mutant strains exhibiting long-chain-base auxotrophy are deficient in serine palmitoyltransferase activity. *J Bacteriol* **174:** 2575-2581.

Portillo F, de Larrinoa IF, Serrano R (1989) Deletion analysis of yeast plasma membrane H+-ATPase and identification of a regulatory domain at the carboxyl-terminus. *FEBS Lett* **247:** 381-385.

Sanders D, Slayman CL (1982) Control of intracellular pH. Predominant role of oxidative metabolism, not proton transport, in the eukaryotic microorganism Neurospora. *J Gen Physiol* **80:** 377-402.

Savageau MA (1969a) Biochemical systems analysis. I. Some mathematical properties of the rate law for the component enzymatic reactions. *J Theor Biol* **25:** 365-369.

Savageau MA (1969b) Biochemical systems analysis. II. The steady-state solutions for an n-pool system using a power-law approximation. *J Theor Biol* **25:** 370-379.

Sawai H, Okamoto Y, Luberto C, Mao C, Bielawska A, Domae N, Hannun YA (2000) Identification of *ISC1* (YER019w) as inositol phosphosphingolipid phospholipase C in *Saccharomyces cerevisiae*. *The Journal of biological chemistry* **275:** 39793-39798.

Serrano R (1988) Structure and function of proton translocating ATPase in plasma membranes of plants and fungi. *Biochim Biophys Acta* **947:** 1-28.

Shi L, Yoon SR, Bezerra AG, Jr., Jung KH, Brown LS (2006) Cytoplasmic shuttling of protons in anabaena sensory rhodopsin: implications for signaling mechanism. *J Mol Biol* **358:** 686-700.

Smit EJ, Kock JL, van der Westhuizen JP, Britz TJ (1988) Taxonomic relationships of Cryptococcus and Tremella based on fatty acid composition and other phenotypic characters. *J Gen Microbiol* **134:** 2849-2855.

Smith SW, Lester RL (1974) Inositol phosphorylceramide, a novel substance and the chief member of a major group of yeast sphingolipids containing a single inositol phosphate. *The Journal of biological chemistry* **249:** 3395-3405.

Soteropoulos P, Vaz T, Santangelo R, Paderu P, Huang DY, Tamas MJ, Perlin DS (2000) Molecular characterization of the plasma membrane H(+)-ATPase, an antifungal target in Cryptococcus neoformans. *Antimicrob Agents Chemother* **44:** 2349-2355.

Torres NV, Voit EO (2002) *Pathway analysis and optimization in metabolic engineering*. Cambridge University Press, Cambridge, U.K.

van der Rest ME, Kamminga AH, Nakano A, Anraku Y, Poolman B, Konings WN (1995) The plasma membrane of Saccharomyces cerevisiae: structure, function, and biogenesis. *Microbiol Rev* **59:** 304-322.

Voit EO (2000) *Computational Analysis of Biochemical System. A practical guide for biochemists and Molecular Biologists*. Cambridge University Press.

Voit EO (2002) Models-of-data and models-of-processes in the post-genomic era. *Math Biosci* **180:** 263-274.

Voit EO, Savageau MA (1987) Accuracy of alternative representations for integrated biochemical systems. *Biochemistry* **26:** 6869-6880.

Wu WI, McDonough VM, Nickels JT, Jr., Ko J, Fischl AS, Vales TR, Merrill AH, Jr., Carman GM (1995) Regulation of lipid biosynthesis in Saccharomyces cerevisiae by fumonisin B1. *The Journal of biological chemistry* **270:** 13171-13178.

SUPPLEMENTARY TABLES

Table S1: Reactions included in the model of sphingolipid metabolism in *Cryptococcus neoformans*.

Reaction	Independent Variable	Activity (μmol/mg/min)	Reference
$\text{Palmitate}(X_{18}) + Ac - CoA(X_{104}) \xrightarrow{X_{131}} \text{Pal} - \text{CoA}(X_1)$	*Palmitoyl-CoA Synthase*	0.050	(Kamiryo *et al*, 1976)
$\text{Pal} - \text{CoA}(X_1) + \text{Serine}(X_2) \xrightarrow{X_{108}} \text{KDHS}(X_3)$	*Serine Palmitoyltransferase*	0.014	(Merrill *et al*, 1988)
$\text{KDHS}(X_3) \xrightarrow{X_{111}} \text{DHS}(X_4)$	*KDHS Reductase*	0.26E-3	(Pinto *et al*, 1992b)
$\text{DHS}(X_4) + C_{24} - CoA(X_{107}) \xrightarrow{X_{112}} \text{Dihydro} - \text{C}_{24}(X_5)$	*DH-Cer-Synthase*	0.16E-4	(Wu *et al*, 1995)
$\text{DHS}(X_4) + C_{26} - CoA(X_{105}) \xrightarrow{X_{112}} \text{Dihydro} - \text{C}_{26}(X_6)$			
$\text{DHS}(X_4) + C_{18} - CoA(X_{106}) \xrightarrow{X_{112}} \text{Dihydro} - \text{C}_{18}(X_7)$			
$\text{Dihydro} - \text{C}_{24}(X_5) \xrightarrow{X_{110}} \text{DHS}(X_4)$	*DH-Ceramidase*	0.54E-5	(Mao *et al*, 2000)
$\text{Dihydro} - \text{C}_{26}(X_6) \xrightarrow{X_{110}} \text{DHS}(X_4)$			
$\text{Dihydro} - \text{C}_{18}(X_7) \xrightarrow{X_{110}} \text{DHS}(X_4)$			
$\text{PHS}(X_8) + C_{24} - CoA(X_{107}) \xrightarrow{X_{116}} \text{Phyto} - \text{C}_{24}(X_{10})$	*Phytoceramide Synthase*	0.16E-4	(Wu *et al*, 1995)
$\text{PHS}(X_8) + C_{26} - CoA(X_{105}) \xrightarrow{X_{116}} \text{Phyto} - \text{C}_{26}(X_9)$			
$\text{PHS}(X_8) + C_{18} - CoA(X_{106}) \xrightarrow{X_{116}} \text{Phyto} - \text{C}_{18}(X_{11})$			
$\text{Phyto} - \text{C}_{26}(X_9) \xrightarrow{X_{113}} \text{PHS}(X_8)$	*Phyto-Ceramidase*	0.198E-4	(Mao *et al*, 2000)
$\text{Phyto} - \text{C}_{24}(X_{10}) \xrightarrow{X_{113}} \text{PHS}(X_8)$			
$\text{Phyto} - \text{C}_{18}(X_{11}) \xrightarrow{X_{113}} \text{PHS}(X_8)$			
$\text{Phyto} - \text{C}_{18}(X_{11}) + PI(X_{120}) \xrightarrow{X_{121}} \text{IPC} - \text{C}_{18}(X_{15}) + \text{DAG}(X_{19})$	*Inositol Phosphorylceramide Synthase*	0.35E-4	(Heung *et al*, 2004)
$\text{Phyto} - \text{C}_{24}(X_{10}) + PI(X_{120}) \xrightarrow{X_{121}} \text{IPC} - \text{C}_{24}(X_{14}) + \text{DAG}(X_{19})$			
$\text{Phyto} - \text{C}_{26}(X_9) + PI(X_{120}) \xrightarrow{X_{121}} \text{IPC} - \text{C}_{26}(X_{13}) + \text{DAG}(X_{19})$			
$\text{DHS}(X_4) \xrightarrow{X_{114}} \text{PHS}(X_8)$	*Hydroxylase*	0.17E-3	(Grilley *et al*, 1998)
$\text{Dihydro} - \text{C}_{26}(X_6) \xrightarrow{X_{115}} \text{Phyto} - \text{C}_{26}(X_9)$	*Hydroxylase*	0.17E-3	(Grilley *et al*, 1998)
$\text{IPC} - C_{26}(X_{13}) \xrightarrow{X_{119}} \text{Phyto} - C_{26}(X_9)$	*Inositol Phosphosphingolipid Phospholipase C*	(*) 0.12E-7	Unpublished data
$Pma1p\ (X_{117}) \xrightarrow{X_{118}} \text{Pma1}(X_{12})$	*Sec61*	(a) 2.06	(Fan *et al*, 2005)
$H^+(X_{126}) \xrightarrow{X_{128}} \text{H}^+(X_{16})$	*H^+ Transport*	(b) 8.5	(Shi *et al*, 2006)
$ADP + P_i + H^+ \xleftrightarrow{X_{135}} \text{ATP}(X_{17}) + H_2O$	*F_1F_0 -ATP synthase*	(c) 5.62	(Akhter *et al*, 2003;
$NADH_m(X_{123}) + O_2(X_{124}) \xrightarrow{X_{122}} NAD_m$	*Alternative Respiration*	0.15E-4	Arselin *et al*, 2003)
$\text{ATP}(X_{17}) + \text{H}^+(X_{16}) \xrightarrow{X_{125}} ADP(X_9) + H^+(X_{126})$	*H^+-ATPase*	0.05	(Portillo *et al*, 1989)
$Palmitate\ Ext.(X_{100}) \xrightarrow{X_{102}} \text{Palmitate}(X_{18})$	*Palmitate Transport*	(d) 3.11E-3	(Faergeman & Knudsen, 1997)
$Serine\ Ext.(X_{101}) \xrightarrow{X_{103}} \text{Serine}(X_2)$	*Serine Transport*	0.0092	(Fein & MacLeod, 1975)

(*) μmol hydrolyzed IPC/ mg protein /min; (a) Fold change see Table S8; (b) H^+ permeability value reported as (μm/min); (c) Activity of F_1F_0 ATP synthase by fold change, see Table S8 and text, (d) Value reported as (μmol/min 10^8 cells).

Table S2: Proton flux data for *C. neoformans*.

Parameter	Value	Reference
Melanin thickness	0.16 (μm)	(Eisenman *et al*, 2005)
H^+ permeability	8.5 (μm/min)	(Shi *et al*, 2006)
Cytoplasmatic volume	51.5 μm^3	(Garcia-Rivera *et al*, 2004)
Z potential	-24.42 (mV)	(Nosanchuk & Casadevall, 1997)
Capsule thickness	5.41 (μm)	(Garcia-Rivera *et al*, 2005)
H^+ ext. conc.	31 (μM/l)	$pH_{ext.}$=4.5
H^+ int. conc.	0.31 (μM/l)	pH_i=6.5

Table S3: Rate laws governing the sphingolipid model (symbolic form)

$V_1^+ : v_{18,1} = V_{max}\left[\left(X_{18}/K_{M,Palmitate} + X_{18}\right)\left(X_{104}/K_{M,Ac-CoA} + X_{104}\right)\right]$;

$V_1^- : v_{1,3} = V_{max}\left[\left(X_1/K_{M,Pal-CoA} + X_1\right)\left(X_2/K_{M,Serine-CoA} + X_2\right)\right]$;

$V_2^+ : v_{101,2} = \left(V_{max} \cdot X_{101}/K_{M,Serine} + X_{101}\right)$;

$V_2^- : v_{1,3}; \quad v_{2,129} = \left(V_{max} \cdot X_2/K_{M,SHMT} + X_2\right)$

$V_3^+ : v_{1,3}$;

$V_3^- : v_{3,4} = \left(V_{max} \cdot X_3/K_{M,KDHS} + X_3\right)$;

$V_4^+ : v_{3,4}; \quad v_{5,4} = \left(V_{max} \cdot X_5/K_{M,Dihydro-C_{24}} + X_5\right)$;

$v_{6,4} = \left(V_{max} \cdot X_6/K_{M,Dihydro-C_{26}} + X_6\right) \quad v_{7,4} = \left(V_{max} \cdot X_7/K_{M,Dihydro-C_{18}} + X_7\right)$;

$V_4^- : v_{4,5} = V_{max}\left[\left(X_4/K_{M,DHS} + X_4\right)\left(X_{107}/K_{M,C_{24}-CoA} + X_{107}\right)\right]; \quad v_{4,6} = V_{max}\left[\left(X_4/K_{M,DHS} + X_4\right)\left(X_{105}/K_{M,C_{26}-CoA} + X_{105}\right)\right]$;

$v_{4,7} = V_{max}\left[\left(X_4/K_{M,DHS} + X_4\right)\left(X_{106}/K_{M,C_{18}-CoA} + X_{106}\right)\right]; \quad v_{4,8} = \left(V_{max} \cdot X_4/K_{M,DHS} + X_4\right)$;

$V_5^+ : v_{4,5}$;

$V_5^- : v_{5,4}$;

$V_6^+ : v_{4,6}$;

$V_6^- : v_{6,9} = \left(V_{max} \cdot X_6/K_{M,Dihydro-C_{26}} + X_6\right)$; $v_{6,4}$;

$V_7^+ : v_{4,7}$;

$V_7^- : v_{7,4}$;

$V_8^+ : v_{9,8} = \left(V_{max} \cdot X_9/K_{M,Phyto-C_{26}} + X_9\right)$; $v_{11,8} = \left(V_{max} \cdot X_{11}/K_{M,Phyto-C_{18}} + X_{11}\right)$;

$V_8^- : v_{8,9} = V_{max}\left[\left(X_8/K_{M,PHS} + X_8\right)\left(X_{105}/K_{M,C_{26}-CoA} + X_{105}\right)\right]$; $v_{10,8} = \left(V_{max} \cdot X_{10}/K_{M,Phyto-C_{24}} + X_{10}\right)$;

$v_{8,10} = V_{max}\left[\left(X_8/K_{M,PHS} + X_8\right)\left(X_{107}/K_{M,C_{24}-CoA} + X_{107}\right)\right]$; $v_{8,11} = V_{max}\left[\left(X_8/K_{M,PHS} + X_8\right)\left(X_{106}/K_{M,C_{18}-CoA} + X_{106}\right)\right]$;

$V_9^+ : v_{8,9}; \quad v_{13,9} = \left(V_{max} \cdot X_{13}/K_{M,IPC-C_{26}} + X_{13}\right)$;

$V_9^- : v_{9,8}; \; v_{9,13} = V_{max}\left[\left(X_9/K_{M,Phyto-C_{26}} + X_9\right)\left(X_{120}/K_{M,PI} + X_{120}\right)\right]$;

$V_{10}^+ : v_{8,10} = V_{max}\left[\left(X_8/K_{M,PHS} + X_8\right)\left(X_{107}/K_{M,C_{24}-CoA} + X_{107}\right)\right]$;

V_{10}^{-}: $v_{10,14} = V_{max}\left[\left(X_{10}/K_{M,IPC-C_{24}} + X_{10}\right)\left(X_{120}/K_{M,PI} + X_{120}\right)\right]$

V_{11}^{+}: $v_{8,11}$;

V_{11}^{-}: $v_{11,8}$; $v_{11,15} = V_{max}\left[\left(X_{11}/K_{M,IPC-C_{18}} + X_{11}\right)\left(X_{120}/K_{M,PI} + X_{120}\right)\right]$;

V_{12}^{+}: $v_{117,12} = V_{max,ATPase} \cdot [mRNA]$ *(Probable endoplasmic reticulum insertion protein SEC61);*

V_{12}^{-}: $v_{12,12} = X_{12} \cdot [mRNA]$ *(Potential phospholipids transporting ATPase);*

V_{13}^{+}: $v_{9,13}$;

V_{13}^{-}: $v_{13,9}$;

V_{14}^{+}: $v_{10,14}$;

V_{14}^{-}: $v_{14,130}$;

V_{15}^{+}: $v_{11,15}$;

V_{15}^{-}: $v_{15,130}$;

V_{16}^{+}: $v_{126,16} = (H_p^{+} \cdot C_t \cdot M_t \cdot P_c / V)$;

V_{16}^{-}: $v_{16,125} = V_{max} \cdot X_{16} \Big/ X_{16} + K_{M,ATP} \cdot \left(1 + \dfrac{[H^{+}]}{K_{s,ATP}}\right)$;

V_{17}^{+}: $v_{135,17} = \left(V_{max} \cdot X_{ADP} / K_{M,ADP} + X_{ADP}\right)$

V_{17}^{-}: $v_{17,125} = V_{max} \cdot X_{17} \Big/ X_{17} + K_{M,ATP} \cdot \left(1 + \dfrac{[H^{+}]}{K_{s,ATP}}\right)$;

V_{18}^{+}: $v_{100,18} = (V_{max} \cdot X_{100} / K_{M,Palmitate\ Ext.} + X_{100})$;

V_{18}^{-}: $v_{18,1}$;

V_{19}^{+}: $v_{9,13}, v_{10,14}, v_{11,15}$;

V_{19}^{-}: $v_{19,130} : X_{130}$

Table S4: Nominal steady-state values for concentrations and fluxes in the sphingolipid model for *Cryptococcus neoformans* (see Figure 1 for pathway representation).

Variable number (X_i)	Variable name	Concentration	Reference	Flux (μM/min/l)
1	Pal-CoA	0.2 μM	(Knudsen *et al*, 1999)	0.14
2	Serine	2.6 μM	(Kelley *et al*, 1988)	1.38
3	KDHS	3 μM	(Kihara & Igarashi, 2004)	0.14
4	DHS	[(a)] 0.05	this work	1.59
5	Dihydro-C_{24}	[(a)] 0.0 37	this work	0.63
6	Dihydro-C_{26}	[(a)] 0.136	this work	0.45
7	Dihydro-C_{18}	[(a)] 0.062	this work	0.39
8	PHS	[(a)] 0.089	this work	0.15
9	Phyto-C_{26}	[(a)] 0 .166	this work	4.34
10	Phyto-C_{24}	[(a)] 0.29	this work	0.14
11	Phyto-C_{18}	[(a)] 0.158	this work	1.0E-2
12	Pma1	[(b)] 0.103	(Portillo *et al*, 1989)	0.10
13	IPC-C_{26}	[(c)] 2.257	(Hechtberger *et al*, 1994; Smith & Lester, 1974)	4.30
14	IPC-C_{24}	[(c)] 0.396	(Hechtberger *et al*, 1994; Smith & Lester, 1974)	0.14
15	IPC-C_{18}	[(c)] 0.396	(Hechtberger *et al*, 1994; Smith & Lester, 1974)	2.4E-3
16	H^+	[(d)] 0.31 μM	this work	4.49
17	ATP	0.82E-7 μmol /mg protein	this work	9.7E-5
18	Palmitate	0.2 μM	(Knudsen *et al*, 1999)	0.14
19	DAG	0.0249 μmol / ρmol P_i	this work	4.44

Total protein concentrations were determined at 24 hours of growth, for *pH*= 6.2 and YPD medium conditions as 401, 42 mg/l.

[(a)] Normalized sphingolipid concentration; [(b)] Activity of H^+ATPase (μM/mg/min) include the fold change (probable endoplasmic reticulum insertion protein SEC-61), see Table S8 (Fan *et al*, 2005). **[(c)] See section 1.4. [(d)] Calculated as $10^{(-pHext)}$.**

Table S5: *Eigenvalues* of the sphingolipid model for *Cryptococcus neoformans*.

(min^{-1})
-0.1770911
-0.0003041061
-89.30528
-343.6299
-34.81049
-24.39046
-5.73124
-2.371997
-0.1642581
-1.208335
-0.005620033
-0.9001784
-0.008645724
-14.488
-1
-0.3414943
-0.4903173
-0.03902694
-0.6955297

At the nominal steady state, all *eigenvalues* of the system have negative real parts, confirming local stability. The magnitudes of the real parts give an indication of the relative time scales that are represented in the model. The largest magnitude is -89.305 min^{-1} and the smallest magnitude is -0.000306 min^{-1}.

Table S6: **Symbolic GMA representation of our sphingolipid model in *Cryptococcus neoformans* (see Figure 1 in main text for the pathway diagram).**

$$dX_1/dt = \alpha_{1,18} X_{18}^{g_{1,18,18}} X_{104}^{g_{1,104,18}} X_{131}^{g_{1,131,18}} - \beta_{1,3} X_1^{h_{1,1,3}} X_2^{h_{1,2,3}} X_{108}^{h_{1,108,3}}$$

$$dX_2/dt = \alpha_{2,101} X_{103}^{g_{2,103,101}} X_{101}^{g_{2,101}} - \beta_{2,3} X_1^{h_{2,1,3}} X_2^{h_{2,2,3}} X_{108}^{h_{2,108,3}} - \beta_{2,2} X_2^{h_{2,2,2}} X_{129}^{h_{2,129,2}}$$

$$dX_3/dt = \alpha_{3,1} X_1^{g_{3,1,1}} X_2^{g_{3,2,1}} X_{108}^{g_{3,108,1}} - \beta_{3,4} X_3^{h_{3,3,4}} X_{111}^{h_{3,111,4}}$$

$$dX_4/dt = \alpha_{4,3} X_3^{g_{4,3,3}} X_{111}^{g_{4,111,3}} + \alpha_{4,5} X_5^{g_{4,5,5}} X_{110}^{g_{4,110,5}} + \alpha_{4,6} X_6^{g_{4,6,6}} X_{110}^{g_{4,110,6}} + \alpha_{4,7} X_7^{g_{4,7,7}} X_{110}^{g_{4,110,7}}$$
$$- \beta_{4,5} X_4^{h_{4,4,5}} X_{107}^{h_{4,107,4,5}} X_{112}^{h_{4,112,5}} - \beta_{4,6} X_4^{h_{4,4,6}} X_{105}^{h_{4,105,6}} - \beta_{4,7} X_{106}^{h_{4,106,7}} X_{114}^{h_{4,114,7}}$$

$$dX_5/dt = \alpha_{5,4} X_4^{g_{5,4,4}} X_{107}^{g_{5,107,4}} X_{112}^{g_{5,112,4}} - \beta_{5,5} X_5^{h_{5,5}} X_{110}^{h_{5,110,5}}$$

$$dX_6/dt = \alpha_{6,4} X_4^{g_{6,4,4}} X_{105}^{g_{6,105,4}} X_{112}^{g_{6,112,4}} - \beta_{6,4} X_6^{h_{6,6,4}} X_{110}^{h_{6,110,4}} - \beta_{6,9} X_6^{h_{6,6,9}} X_{115}^{h_{6,115,9}}$$

$$dX_7/dt = \alpha_{7,4} X_4^{g_{7,4,4}} X_{106}^{g_{7,106,4}} X_{112}^{g_{7,112,4}} - \beta_{7,4} X_7^{h_{7,7,4}} X_{110}^{h_{7,110,4}}$$

$$dX_8/dt = \alpha_{8,4} X_4^{g_{8,4,4}} X_{113}^{g_{8,113,4}} X_{114}^{g_{8,114,4}} + \alpha_{8,9} X_9^{g_{8,9,9}} X_{113}^{g_{8,113,9}} + \alpha_{8,10} X_{10}^{g_{8,9,10}} X_{113}^{g_{8,113,10}} + \alpha_{8,11} X_{11}^{g_{8,11,11}} X_{113}^{g_{8,113,11}}$$
$$- \beta_{8,9} X_8^{h_{8,8,9}} X_{105}^{h_{8,105,9}} X_{116}^{h_{8,116,9}} - \beta_{8,10} X_8^{h_{8,8,10}} X_{107}^{h_{8,107,10}} X_{116}^{h_{8,116,10}} - \beta_{8,11} X_8^{h_{8,8,11}} X_{106}^{h_{8,106,11}} X_{116}^{h_{8,116,11}}$$

$$dX_9/dt = \alpha_{9,6} X_6^{g_{9,6,6}} X_{115}^{g_{9,115,6}} + \alpha_{9,8} X_8^{g_{9,8,8}} X_{105}^{g_{9,105,8}} X_{116}^{g_{9,116,8}} + \alpha_{9,13} X_{13}^{g_{9,13,13}} X_{119}^{g_{9,119,13}} X_{134}^{g_{9,134,13}}$$
$$- \beta_{9,13} X_9^{h_{9,121,13}} X_{120}^{h_{9,120,13}} X_{121}^{h_{9,121,13}} X_{127}^{h_{9,127,13}} - \beta_{9,8} X_9^{h_{9,9,8}} X_{113}^{h_{9,113,8}}$$

$$dX_{10}/dt = \alpha_{10,8} X_8^{g_{10,8,8}} X_{107}^{g_{10,107}} X_{116}^{g_{10,116}} - \beta_{10,14} X_{10}^{h_{10,10,14}} X_{113}^{h_{10,113,14}} X_{120}^{h_{10,120,14}} X_{121}^{h_{10,121,14}} X_{127}^{h_{10,127,14}}$$

$$dX_{11}/dt = \alpha_{11,8} X_8^{g_{11,8,8}} X_{106}^{g_{11,106,8}} X_{116}^{g_{11,116,8}} - \beta_{11,8} X_{11}^{h_{11,11,8}} X_{113}^{h_{11,113,8}} - \beta_{11,15} X_{11}^{h_{11,11,15}} X_{120}^{h_{11,120,15}} X_{121}^{h_{11,121,15}} X_{127}^{h_{11,127,15}}$$

$$dX_{12}/dt = \alpha_{12} X_9^{g_{12,9}} X_{13}^{g_{12,13}} X_{117}^{g_{12,117}} X_{118}^{g_{12,118}} X_{119}^{g_{12,119}} X_{121}^{g_{12,121}} - \beta_{12} X_{12}^{h_{12,12}} X_{125}^{h_{12,125}}$$

$$dX_{13}/dt = \alpha_{13,9} X_9^{g_{13,9,9}} X_{120}^{g_{13,120,9}} X_{121}^{g_{13,121,9}} X_{127}^{g_{13,127,9}} - \beta_{13,9} X_{13}^{h_{13,13,9}} X_{119}^{h_{13,119,9}} X_{134}^{h_{13,134,9}}$$

$$dX_{14}/dt = \alpha_{14,10} X_{10}^{g_{14,10,10}} X_{120}^{g_{14,120,10}} X_{121}^{g_{14,121,10}} X_{127}^{g_{14,127,10}} - \beta_{14,14} X_{14}^{h_{14,14}} X_{130}^{h_{14,130}}$$

$$dX_{15}/dt = \alpha_{15,11} X_{11}^{g_{15,11,11}} X_{120}^{g_{15,120,11}} X_{121}^{g_{15,121,11}} X_{127}^{g_{15,12,11}} - \beta_{15,15} X_{15}^{h_{15,15}} X_{130}^{h_{15,130}}$$

$$dX_{16}/dt = \alpha_{16,126} X_{126}^{g_{16,126}} X_{128}^{g_{16,128,126}} - \beta_{16,125} X_{12}^{h_{16,12,125}} X_{16}^{h_{16,16,125}} X_{17}^{h_{16,17,125}} X_{125}^{h_{16,125}}$$

$$dX_{17}/dt = \alpha_{17,135} X_{17}^{g_{17,17,135}} X_{119}^{g_{17,119,135}} X_{122}^{g_{17,122,135}} X_{123}^{g_{17,123,135}} X_{124}^{g_{17,124,135}} X_{132}^{g_{17,132,135}} X_{135}^{g_{17,135}} X_{136}^{g_{17,136,135}}$$
$$- \beta_{17,125} X_{16}^{h_{17,16,125}} X_{17}^{h_{17,17,125}} X_{125}^{h_{17,125}} - \beta_{17,135} X_{17}^{h_{17,17,135}} X_{132}^{h_{17,132,135}} X_{135}^{h_{17,135}} X_{136}^{h_{17,136,135}}$$

$$dX_{18}/dt = \alpha_{18,100} X_{102}^{g_{18,102,100}} X_{100}^{g_{18,100}} - \beta_{18,1} X_{18}^{h_{18,18,1}} X_{131}^{h_{18,131,1}} X_{104}^{h_{18,104,1}}$$

$$dX_{19}/dt = \alpha_{19,9} X_9^{g_{19,9,9}} X_{120}^{g_{19,120,9}} X_{121}^{g_{19,121,9}} + \alpha_{19,10} X_{10}^{g_{19,10,10}} X_{120}^{g_{19,120,10}} X_{121}^{g_{19,121,10}}$$
$$+ \alpha_{19,11} X_{11}^{g_{19,11,11}} X_{120}^{g_{19,120,11}} X_{121}^{g_{19,121,11}} - \beta_{19,130} X_{130}^{h_{19,130}} X_{19}^{h_{19,19}}$$

Table S7: Numerical S-system representation of our sphingolipid model in *Cryptococcus neoformans* (see Figure 1 in main text for the pathway diagram).

$$dX_1/dt = 3.003\, X_{18}^{0.979} X_{104}^{0.514} X_{131} - 20.959\, X_1^{0.5} X_2^{0.071} X_{108}$$

$$dX_2/dt = 7.526\, X_{101}^{0.5} X_{103} - 125.677\, X_1^{0.050} X_2^{0.902} X_{108}^{0.101} X_{129}^{0.898}$$

$$dX_3/dt = 20.959\, X_1^{0.50} X_2^{0.071} X_{108} - 214.666\, X_3^{0.833} X_{111}$$

$$dX_4/dt = 684{,}088.19 X_3^{0.0736} X_5^{0.199} X_6^{0.136} X_7^{0.125} X_{110}^{0.911} X_{111}^{0.088} - 402{,}718.59 X_4^{0.950} X_{105}^{0.261} X_{106}^{0.250} X_{107}^{0.398} X_{112}^{0.933} X_{114}^{0.066}$$

$$dX_5/dt = 497{,}688.05\, X_4^{0.983} X_{107} X_{112} - 609{,}367.99\, X_5^{0.49} X_{110}$$

$$dX_6/dt = 172{,}842.41\, X_4^{0.983} X_{105}^{0.918} X_{112} - 175{,}393.72\, X_6^{0.5} X_{110}^{0.924} X_{115}^{0.0753}$$

$$dX_7/dt = 19{,}144.71\, X_4^{0.983} X_{106} X_{112} - 295{,}927.42\, X_7^{0.5} X_{110}$$

$$dX_8/dt = 6{,}324.95\, X_4^{0.350} X_9^{0.134} X_{10}^{0.0130} X_{11}^{0.0075} X_{113}^{0.299} X_{114}^{0.7} - 146{,}870.61\, X_8^{0.692} X_{105}^{0.018} X_{106}^{0.0005} X_{107}^{0.552} X_{116}$$

$$dX_9/dt = 0.656 \times 10^8\, X_6^{0.0030} X_8^{0.00082} X_{13}^{0.501} X_{105}^{0.0005} X_{115}^{0.0061} X_{116}^{0.001} X_{119}^{0.992} X_{134}^{0.992} - 0.135 \times 10^8\, X_9^{0.887} X_{113}^{0.007} X_{120}^{0.227} X_{121}^{0.99} X_{127}^{0.992}$$

$$dX_{10}/dt = 144{,}078.091\, X_8^{0.692} X_{107}^{0.581} X_{116} - 445{,}613.551\, X_{10}^{1.864} X_{113}^{0.763} X_{120}^{0.0079} X_{121}^{0.972} X_{127}^{0.972}$$

$$dX_{11}/dt = 308.335\, X_8^{0.692} X_{116} X_{106}^{0.078} - 7.99\, X_{11}^{1.343} X_{113}^{0.763} X_{120}^{0.083} X_{121}^{-0.236} X_{127}^{0.236}$$

$$dX_{12}/dt = 0.612 \times 10^{13}\, X_9^{0.890} X_{13}^{0.504} X_{117} X_{118} X_{119} X_{121} - 0.047\, X_{12} X_{125}$$

$$dX_{13}/dt = 0.107 \times 10^8\, X_9^{0.890} X_{120}^{0.229} X_{121} X_{127} - 0.945 \times 10^8\, X_{13}^{0.612} X_{119} X_{134}$$

$$dX_{14}/dt = 478{,}441.56\, X_{10}^{1.903} X_{120}^{0.524} X_{121} X_{127} - 0.0749\, X_{14}^{0.5} X_{130}$$

$$dX_{15}/dt = 0.735 \times 10^{-6}\, X_{11}^{0.968} X_{120}^{0.355} X_{121}^{-1} X_{127} - 0.000382\, X_{15}^{0.5} X_{130}$$

$$dX_{16}/dt = 0.017\, X_{126} X_{128} - 0.343 \times 10^{11}\, X_{12} X_{17} X_{16}^{0.999} X_{125}$$

$$dX_{17}/dt = 0.296 \times 10^{12}\, X_{17}^{-1.829} X_{119} X_{122} X_{123}^{0.5} X_{124}^{0.5} X_{132}^{2.829} X_{135} - 0.859 \times 10^{11}\, X_{12}^{0.000052} X_{16}^{0.000051} X_{17}^{0.99} X_{125}^{0.000052} X_{132}^{0.999} X_{135}^{0.99}$$

$$dX_{18}/dt = 2.026\, X_{100}^{0.55} X_{102} - 3.003\, X_{18}^{0.99} X_{104}^{0.514} X_{131}$$

$$dX_{19}/dt = 0.112 \times 10^8\, X_9^{0.868} X_{10}^{0.047} X_{11}^{0.000045} X_{120}^{0.236} X_{121} X_{127} - 28.184\, X_{19}^{0.49} X_{130}$$

Table S8: Fold changes in selected genes as determined by microarray analysis for 2 and 24 hours of growth (adapted from (Fan *et al*, 2005)**).**

Gene identification	DMEM vs. MACRO 2 hours	DMEM vs. MACRO 24 hours	Annotation
11P26-B12	0.39	1.58	Potential phospholipid transporting ATPase 1 (EC.3.6.31)
11P52-C12	0.94	1.01	Plasma membrane H^+ATPase
MJB17	0.83	4.68	Ipc1p
11P67-F02	0.95	2.06	Probable endoplasmic reticulum insertion protein Sec61
11P55-C02	1.12	1.07	Mitochondrial ATP synthase (EC. 3.6.3.14)

DMEM: media control.

Macro: macrophage phagocytosed.

Table S9. PLAS file of the model in Figure 1.

Differential equations:	Values of independent variables:	Abbreviation	References
Crryptococcus neoformans_model_Pma1			
X1' =3.003131057*X104^.5141388175*X18^.9900990100*X131^1.- 20.95960359*X1^.5000000003*X2^.7142857119e-1*X108^1.	X100 = 500 X101 = 400	Palmitate Ext Serine Ext	(Lodge *et al*, 1994) (Heung *et al*, 2004)
X2'=7.526625002*X101^.5000000000*X103^1.- 125.6777989*X2^.9022172187*X129^.8985507246*X1^.5072463771e- 1*X108^.1014492754	X102 = .31e-2 X103 = .92e-2 X104 = 18.9	Palmitate Transport Serine Transport Ac-CoA	(Faergeman & Knudsen, 1997) (Faergeman & Knudsen, 1997) (Eisenman *et al*, 2005)
X3'=20.95960359*X1^.5000000003*X2^.7142857119e-1*X108^1.- 214.6667167*X3^.8333333338*X111^1.	X105 = .266 X106 = 2.35	C26-CoA C18-CoA	(Guillas *et al*, 2001) (Guillas *et al*, 2001)
X4'=684088.1960*X3^.7362815766e-1*X111^.8835378914e- 1*X5^.1990225983*X110^.9116462106*X6^.1316873575*X7^.1251131495-	X107 = .1438 X108 = .14e-1	C24-CoA Serine Palmitoyltransferase	(Smit *et al*, 1988) (Guillas *et al*, 2001)
402718.5965*X4^.9509541774*X107^.3980451965*X112^.9331035587*X105^.2 616338611*X106^.2502262987*X114^.6689644068e-1	X109 = .82e-7 X110 = .54e-5	ADP DH-Ceramidase	(Merrill *et al*, 1988) ADP Conc.
X5'= 497688.0512*X4^.9832841688*X107*X112^1.- 609367.9902*X5^.4999999998*X110^1.	X111 = .262e-3 X112 = 1.65e-5	KDHS Reductase DH-Cer-Synthase	(Mao *et al*, 2000) (Pinto *et al*, 1992a)
X6'=172842.4149*X112^1.*X4^.9832841684*X105^.9185548069- 175393.7224*X6^.5000000002*X110^.9246666667*X115^.7533333332e-1	X113 = .198e-4 X114 = .17e-3	Phyto-Ceramidase Hydroxylase	(Guillas *et al*, 2001) (Mao *et al*, 2000)
X7'=19144.71048*X112^1.*X4^.9832841692*X106- 295927.4278*X7^.5000000001*X110^1.	X115 = .17e-3 X117 = 3.158	P-Cer-Synthase Pma1p	(Wu *et al*, 1995) (Portillo *et al*, 1989)
X8'= 6324.956593*X4^.3502134851*X114^.7004269704*X9^.1341383719*X113^.299 5730296*X10^.1308344712e-1*X11^.7505594732e-2-	X118 = 2.06 X119 =.12258e-7 X120 = 4.54	Sec61 Isc1 PI	(Fan *et al*, 2005) Unpublished data (Wu *et al*, 1995)
146870.6183*X116^1.000000000*X8^.6920415225*X105^.1871737786e- 1*X107^.5524568042*X106^.5266873793e-3	X121= .35e-4 X122 = .15e-4	Ipc1 Alternative Respiration	(Heung *et al*, 2004) (Akhter *et al*, 2003)
X9'=89672564.99*X116^.1523450820e-2*X8^.1054291224e- 2*X105^.6538415545e-	X123 = 60 X124 = 5	NADHm Oxygen	(Averet *et al*, 2002) (Ohkusu *et al*, 2004)
3*X134^.9906284692*X13^.6069235685*X119^.9906284692*X6^.3924039991e- 2*X115^.7848079983e-2-	X125 = .5e-1 X126 = 31.00	Pma1-H+ATPase H+ external	(Portillo *et al*, 1989) Proton External
10563252.67*X9^.8868417239*X121^.9906284692*X127^.9906284692*X120^.2 270540637*X113^.9371530803e-2	X127 = .40e-1 X128 = 8.5	ER-GOLGI Transport H+ Transport	(Kihara & Igarashi, 2004) (Kihara & Igarashi, 2004)
X10'=144078.0918*X8^.6920415224*X107^.5817335665*X116^1.- 445613.5500*X121^.9724464238*X127^.9724464238*X120^.5096679375*X10^	X129 = .45e-2 X130 = 1	SHMT Golgi Membrane	(Fischl *et al*, 2000b) (Kastanos *et al*, 1997)
1.864970569*X113^.2755357621e-1 X11'=308.3355165*X106^.7843137248e-1*X116^1.*X8^.6920415228-	X131 = .508e-1 X132 = .246 e-6	Pal-CoA Synthase ATP TOTAL	(Kamiryo *et al*, 1976) ATP Total
7.994176833*X127^.2361593461*X120^.8386340426e- 1*X11^1.346373190/X121^.2361593461*X113^.7638406539	X133 =.82e-7 X134 = 2.25	AMP Golgi-ER Transport	AMP Conc. (*)
X12'=.9783575860e11*X117^1.*X118^1.*X13^.6126651791*X119^1.*X9^.8905 013190*X121^1.-20.00000000*X12^1.*X125^1.	X135 = 5.6282 X136 = .1	F1F0-ATPase H+ m	(Arselin *et al*, 2003)** (Matsuyama & Reed, 2000)
X13'=10763004.38*X9^.8905013190*X121^1.*X127^1.*X120^.2292020377- 94540449.91*X134^1.*X13^.6126651791*X119^1.	Transformation:		
X14'=478441.5621*X121^1.*X127^1.*X120^.5241090152*X10^1.903646037- .2228816516*X14^.4999999997*X130^1.	*pHi* = -log[1/10e 6*X16]		
X15'=.7351868839e-6*X127^1.*X120^.3551136368*X11^.9683356791/X121^1.- .3827389525e-3*X15^.4999999999*X130^1.	Solution parameters:		
X16'=.1705568155e-1*X128^1.*X126^1.- .3430447552e11*X16^.9993784639*X17^.9999999997*X12^1.*X125^1.	t0 = 0 // initial time		
X17'= 90948.93162*X123^.5000000000*X124^.5000000000*X119^1.*X136^.33333333 32*X135^1.*X122^1./X17^1.882631579*X132^1.850408163-	tf = 150 // final time		
28.90708496*X16^.6002627304e-4*X17^.9999983601*X12^.6006360474e- 4*X125^.6006360474e-4*X135^.9999399364*X132^.2040693736e-1	hour = 0.1 // report interval		
X18'=2.026844146*X102^1.*X100^.5000000000- 3.003131057*X104^.5141388175*X18^.9900990100*X131^1.			
X19'= 11211242.31*X9^.8623696687*X121^.9998916887*X127^1.000000000*X120^.2 385092334*X10^.6003461069e-1*X11^.5244085700e-4-			
28.18426652*X130^1.*X19^.4999999999			
Initial values: X1 = .2, X2 = 2.6, X3 = 3, X4 = .51e-1, X5 = .37e-1, X6 = .136, X7 = .62e-1, X8 = .89e-1, X9 = .166, X10 = .29, X11 = .158, X12 = .1030, X13 = 2.257, X14 = .396, X15 = .396, X16 = .31, X17 = .82e-7, X18 = .2, X19 = .249e-1			

Initial values are given for dependent and independent variables; slashes (//) and references are interpreted in PLAS as comments. *Assumed similar to substrate concentration. **Determined based on fold change Ref. (Fan *et al*, 2005)**.**

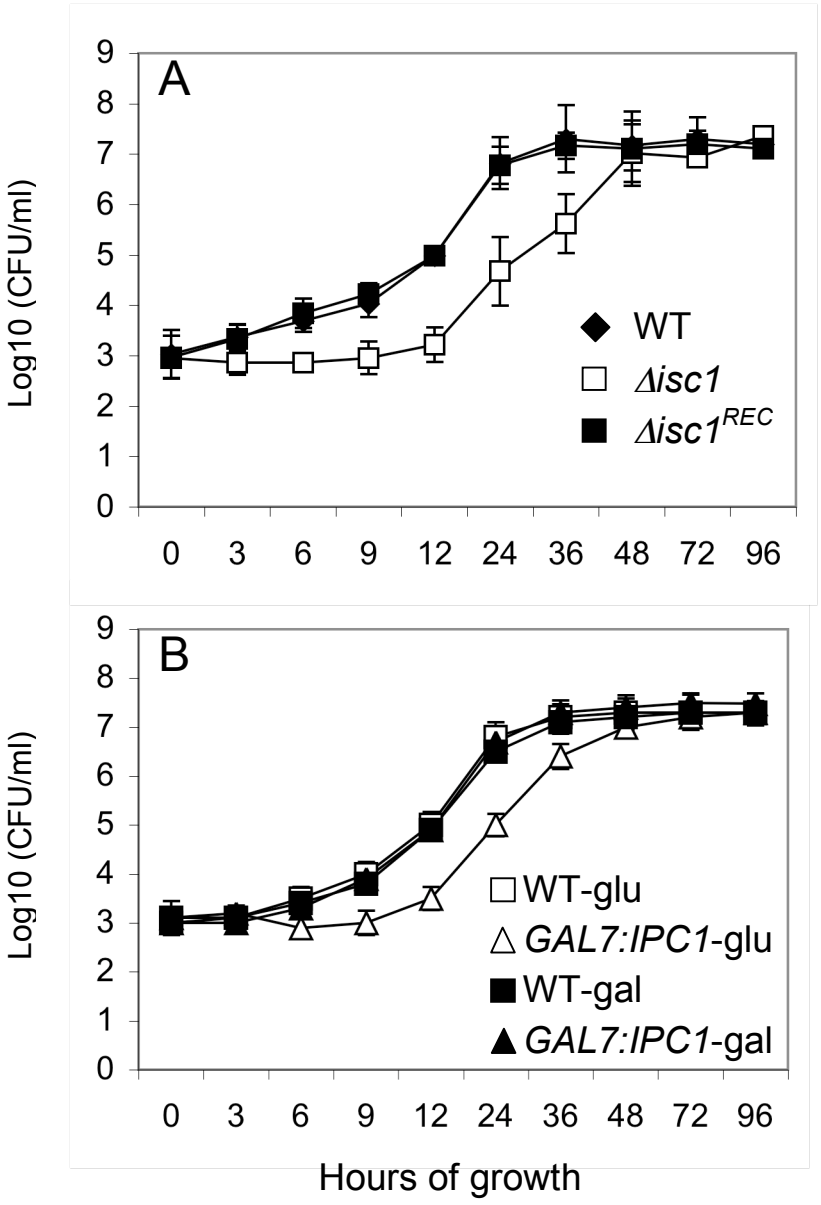

Figure S1: Growth of *C. neoformans* strains defective in the sphingolipid pathway is impaired under acidic conditions. *In vitro* growth curves of *Δisc1* mutant (A), *GAL7::IPC1* (B), and control strains at low *pH* over a period of 96 hours. Abbreviations: Isc1, inositol sphingophospholipid phospholipase C; Ipc1, inositol phosphoryl ceramide synthase; GAL7, Galactose inducible promoter; glu, glucose; gal, galactose.

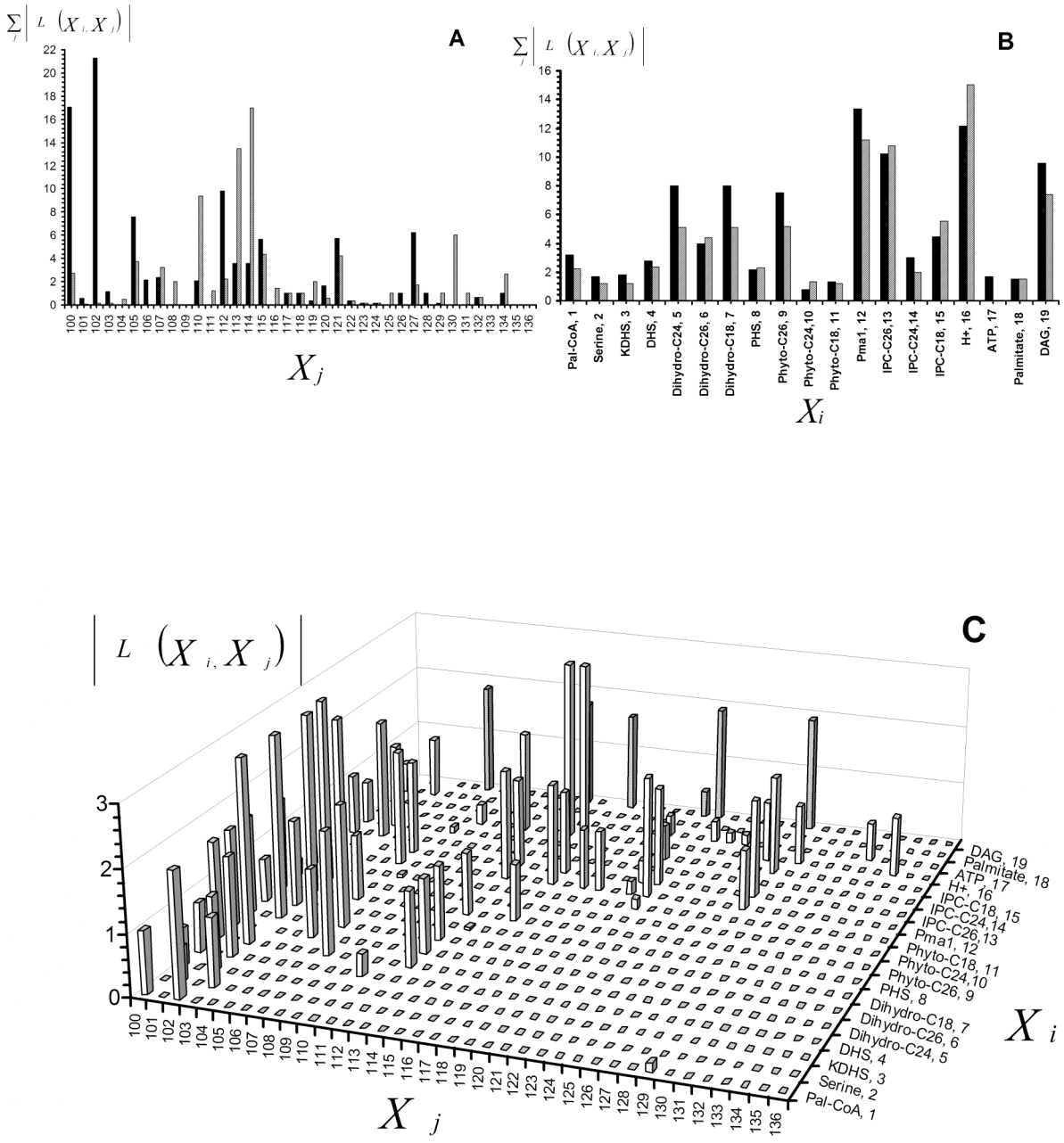

Figure S2: Effects of changes in independent variables on metabolite concentrations as determined by magnitudes of logarithmic gains. The two-dimensional projection **(A)** shows the magnitudes for a particular independent variable summed over all the metabolite concentration. The two-dimensional projection **(B)** shows the magnitudes for a particular metabolite concentration, summed over all independent variables. The three-dimensional plot **(C)** displays the magnitudes of the logarithmic gains as a function of the fluxes and the independent variables. The black and gray bars in each projection represent the sum of positive and negative sensitivities, respectively.

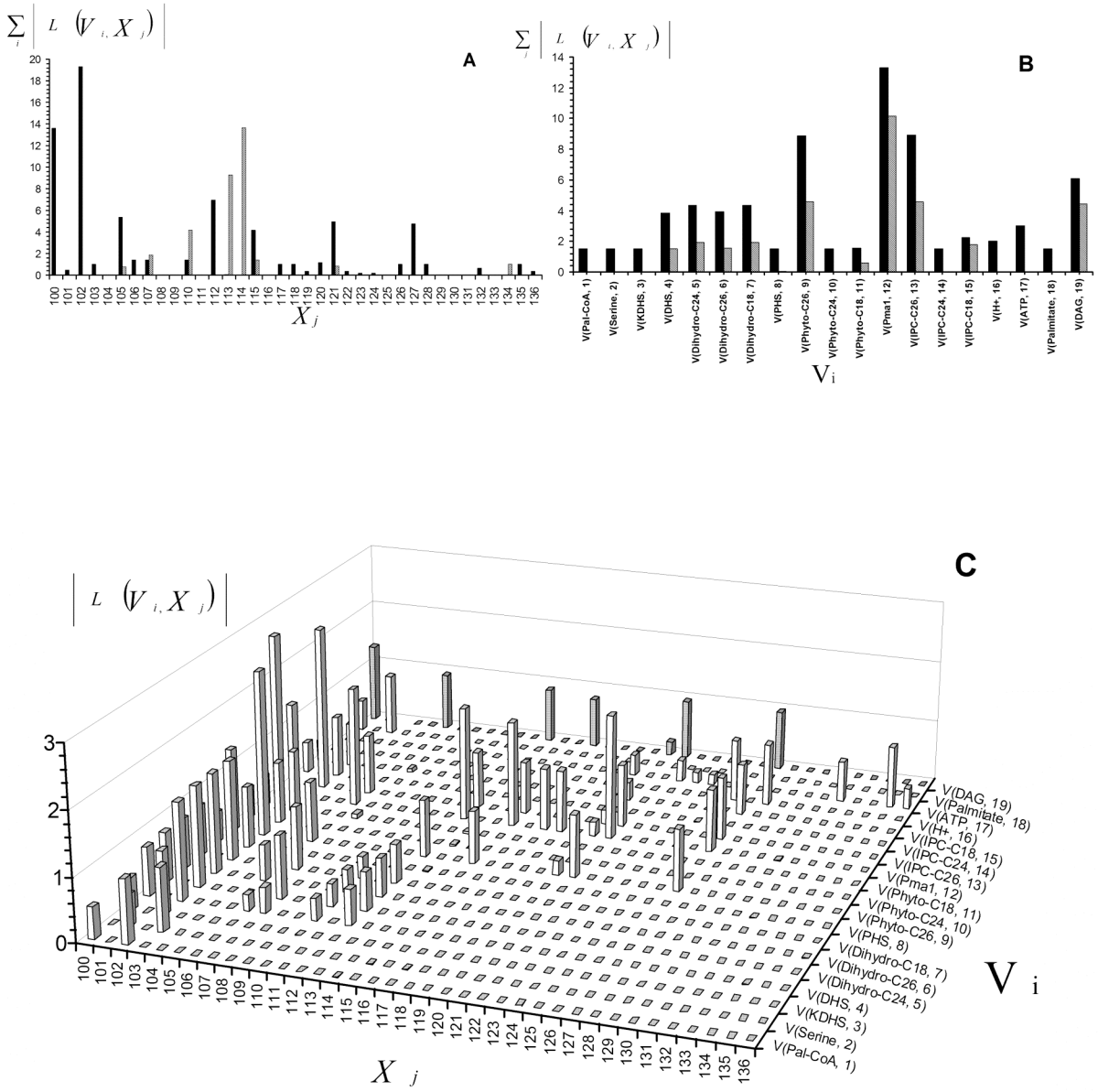

Figure S3: Effects of changes in independent variables on fluxes as determined by magnitudes of logarithmic gains. The two-dimensional projection **(A)** shows the magnitudes for a particular independent variable summed over all the fluxes. **(B)** shows the magnitudes for a particular flux, summed over all independent variables. The three-dimensional plot **(C)** displays the magnitudes of the logarithmic gains as a function of the fluxes and the independent variables. The black and gray bars in each projection represent the sum of positive and negative sensitivities, respectively.